Chemical Science

Accepted Manuscript

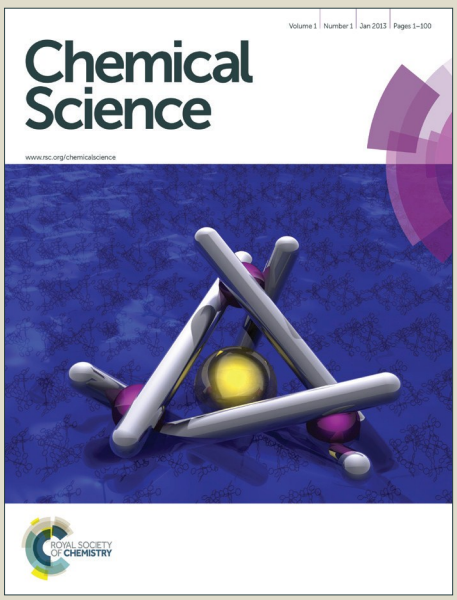

ROYAL SOCIETY OF CHEMISTRY

www.rsc.org/chemicalscience

Journal Name

ARTICLE

Direct and Multiplex Quantification of Protein Biomarkers in Serum Sample with Immuno-magnetic Platform

Received 00th January 20xx,
Accepted 00th January 20xx

DOI: 10.1039/x0xx00000x
www.rsc.org/

See-Lok Ho[a,b], Di Xu[a,b], Man Shing Wong[a,*], Hung-Wing Li[a,*]

A direct and ultrasensitive multiplex assay using an immuno-magnetic platform has been developed for quantification of trace amount of circulating cancer-associated antigens in serum. The detection is based on the specific immuno-interactions among the target antigen, detection antibody and capture antibody that immobilized on the surface of a magnetic nanoparticle. The sandwiched immuno-assembly is then labelled with turn-on fluorophores and detected with a fluorescence imaging system. To afford a high signal-to-noise ratio, three turn-on fluorophores with unique optical property have been designed and synthesized to label the target antigens. The developed assay has achieved a remarkable LOD down to the femto-molar regime without sample pre-treatment. This versatile assay can efficiently differentiate the target antigen from protein matrix and simultaneously quantify multiple cancer-associated antigens, for instance, alpha-fetoprotein (AFP), carcinoembryonic antigen (CEA), and prostate specific antigen (PSA) using only 6 µL of serum sample in an hour. This novel system has a high applicability to serve as a universal and useful tool for early disease diagnostics.

Introduction

In the past decade, protein biomarkers have attracted great interests on early disease diagnosis including cancers, inflammation and neurodegenerative diseases.[1-3] As circulating protein biomarkers, like cancer specific antigens, are found in a wide range of body fluids (liquid biopsy) and the changes in their expression profile is highly correlated to the occurrence and malignancy of a particular cancer,[4-7] these biomarkers are considered as a non-invasive tool for early cancer diagnosis.[8, 9] Cancer development, for instance, is a multistage process that involves different biomarkers, simultaneous detection of multiple biomarkers and establishment of an expression profile can therefore certainly enhance the diagnostic accuracy and facilitate early clinical treatment for a higher survival rate.[10, 11] Unfortunately, current standard methods, such as ELISA and immuno-blotting,[12, 13] often require cumbersome multiple purification and pre-treatment processes and more importantly, these assays are at best only semi-quantitative. Furthermore, to quantify the trace amount of biomarkers in the complex sample matrix, like serum, these standard methods often require a large amount of sample. These problems often hinder the accuracy and the throughput of the assays, and hence limit the clinical applications. In contrast, a simple, direct and yet sensitive and specific detection assay will advance the early cancer diagnosis to the next level.

Herein, we have developed an assay for specific multiplex detection of disease-related antigens with three newly developed turn-on cyanine fluorophores namely, **SLAce**, **SPAce**, and **VLAce.** Cyanine has been reported to be a useful and highly sensitive fluorescence probe that exhibits high binding affinity towards double-stranded DNA and beta-amyloid species.[14, 15] In contrast to the commercially available protein labeling dyes such as FITC, Cy3 and Cy5, these cyanine fluorophores show a strong fluorescence enhancement (> 80-fold) upon binding to the biomolecules, enabling highly sensitive detection of biomarkers. Moreover, the three newly developed dyes being able to be excited by a 488-nm but emitting distinctively different wavelengths facilitates simultaneous detection of multiple target biomarkers under a single excitation light source. Most importantly, the preparation of the cyanine compounds is relatively simple and inexpensive as compared to other organic protein labeling dyes.

For detection, the target analytes are captured and detected on the surface of the nanoparticles based on the specific immuno-interactions between the target antigens and the specific antibodies. A magnetic nanoparticle (MNP) is utilized as the pre-concentration platform for the fact that the magnetic particles can pull the conjugated biomolecules from a laminar path to another by applying an external magnetic field and hence selectively separate the target analytes from the sample matrix without additional offline purification and washing steps.[16-18] Therefore, the magnetic nanoparticle conjugated sandwich immunoassay developed here has

[a] *Department of Chemistry, Hong Kong Baptist University, Hong Kong*
[b] *Contributed equally to this work*
Electronic Supplementary Information (ESI) available: [details of any supplementary information available should be included here]. See DOI: 10.1039/x0xx00000x

offered the advantages of the sandwich immunoassay including the high specificity and binding affinity of the antibody and antigen. In additions, the utility of magnetic nanoparticles allows an online pre-concentration and purification, and hence results in a direct, simple and accurate detection. As a demonstration, three different cancer-associated antigens, alpha-fetoprotein (AFP), carcinoembryonic antigen (CEA), and prostate specific antigen (PSA) were chosen as the target analytes. AFP is a biomarker that well-known to be associated with hepatocellular carcinoma and other malignancies,[19, 20] while abnormal concentrations of CEA and PSA in serum appears to be a sign of colorectal carcinoma[21] and prostate cancer,[22] respectively. The assay was verified to be capable of quantifying the antigens in a serum sample and the result was further validated by ELISA.

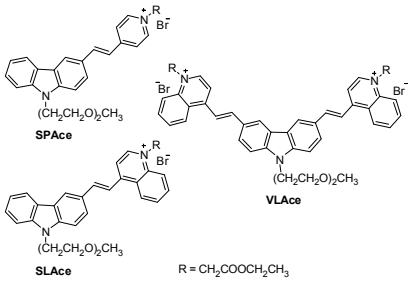

Fig. 1 Molecular structures of the cyanine fluorophores.

Results and discussion

Design of the labelling fluorophore

The molecular structures of the tailor-made cyanine fluorophores are shown in Fig. 1. The syntheses of **SLAce**, **SPAce**, and **VLAce** are outlined in Scheme S1 of the Supporting Information. The cyanine skeleton was synthesized either by the Knoevenagel condensation or the palladium-catalyzed Heck coupling as the key step. The proposed structures were fully characterized by ^{1}H NMR, ^{13}C NMR, and HRMS which are in good agreement with the spectral data. The photophysical properties of these three new cyanines measured in PB solution are summarized in Table S1. They mainly exhibited a very strong and broad charge-transfer absorption band with absorption maximum in the range of 429-524 nm in PB solution. Upon excitation at 488 nm, these cyanines exhibited distinct fluorescence with different emission maximum ranging from 588 to 723 nm. Because of the fast non-radiative decay caused by the strong and dynamic adhesive interactions with water molecules, the fluorescence quantum yields of these cyanines are often low (< 0.1) in PB solution in contrast to the moderate fluorescence obtained in organic solvent such as DMSO. Nevertheless, upon binding with a host, a strong increase in fluorescence will result giving rise to a turn-on fluorescence mechanism for detection of a host. For instance, upon mixing with bovine serum albumin (BSA), there is a strong increase in fluorescence intensity of 7-16 folds for these cyanines. We anticipated that the interaction between proteins and cyanine fluorophores is mainly hydrophobic and π-π stacking interactions as suggested by the blue-shift in emission peak of the fluorophores upon binding to the proteins.

Detection strategy

The detection scheme is illustrated in Fig. 2. Upon the formation of the sandwich immuno-assembly among the capture antibody (Ab1), target antigen, and the detection antibody (Ab2) on the surface of the MNP, the magnetic immuno-assembly (MIA) will be labeled with the tailor-made cyanine fluorophores. The fluorescent MIAs were then introduced into a homemade glass flow cell; The MIAs were then separated from the bulk solution and immobilized on the top coverslip by an external magnetic field. Then, the fluorescent MIAs were visualized and detected under the TIRFM-EMCCD imaging system with a 488 nm cyan excitation laser for quantitative analysis. As the evanescent field generated by the total internal reflection is very shallow, only analytes that locate within the evanescent field are excited by the laser (in this case the MIAs that immobilized at the top coverslip/water interface), while the rest in the bulk solution remains silent. TIRFM improves high signal-to-noise images of the MIAs.

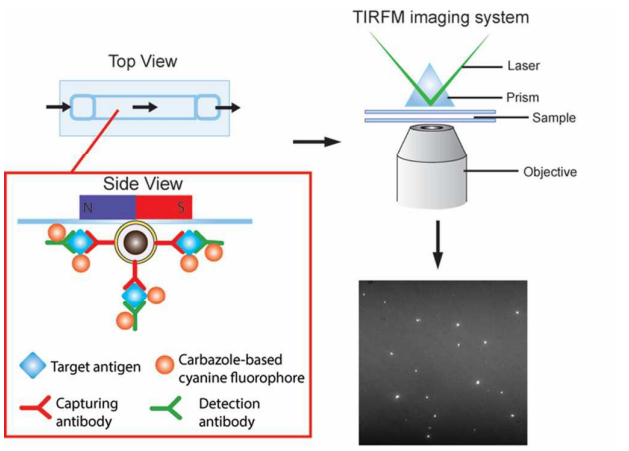

Fig. 2 Schematic illustration of the direct detection of the single sandwiched immuno-assembly with total internal reflection fluorescence microscopy (TIRFM). Silica was coated on the surface of the iron oxide particles by base-catalyzed hydrolysis of tetraethyl orthosilicate (TEOS) in a layer-by-layer assembly fashion. Afterward, the surface of the nanoparticles was further modified by APTES and conjugation of the capture antibody was done by using cross-linker, glutaraldehyde (GA). Target antigen and detection antibodies were added. The sandwiched magnetic immune-assembly (MIA) was labeled by a turn-on cyanine fluorophore. The fluorescence signal of each MIA was recorded and analyzed.

Silica-coated iron oxide nanoparticles were prepared. The TEM (Fig. S1) images revealed that the particles were round in shape and of average diameter 162 ± 25 nm, with average silica shell thickness of 55 ± 6 nm and bare iron oxide nanoparticles of average diameter 5.3 ± 1.0 nm. The as-

prepared MNP dispersed in solution was readily attracted by a small magnet.

For the optimal performance of the detection assay, we firstly studied the concentration dependence of capture antibody that applied to immobilize on surface of the MNP. As depicted in Fig. S2A, the coverage of capture antibody (Ab1) was saturated at the applied concentration of 1 nM as suggested by the highest fluorescence signal obtained from the cyanine, **SLAce**, labeled antibodies conjugated MNPs. Hence Ab1 of concentration 1 nM was applied throughout the entire study. Although the higher population of the MNP immobilized on the flow cell for detection increases the throughput of the assay, the target antigens might distribute themselves among the MNPs and consequently, a "diluted" signal generated. An optimal density of the magnetic nanoparticles can improve the sensitivity of the assay. To study the optimal amount of the MNPs to be applied in the assay, one of the cyanine fluorophores, **SLAce** and PSA are initially chosen as the labeling dye and the target antigen, respectively. As shown in Fig. S2B that the fluorescence signal detected with 20 mg/mL nanoparticles is much lower than 10 mg/mL and 5 mg/mL, it agrees with our prediction that high population of the nanoparticles will weaken the signal generated by the immune-assembly. In addition, the fluorescence signal tends to decrease when the amount of nanoparticles diluted to 5 mg/mL. The low density of the nanoparticles might limit the chance of the target reaches the detection platform, and hence less target will be captured on the nanoparticles. In order to obtain a sensitive detection of the target PSA, 10 mg/mL of the magnetic nanoparticles was applied for the rest of the experiments. To further optimize the performance of the system with respect to the applied concentration of the labeling fluorophores, as illustrated in Fig. S2C, the net intensity of single MIA was highly correlated to the final concentration of the dye from 10 nM to 100 μM. Beyond 100 μM, the increasing amount of the dye was expected to enhance the signal generated, but the background fluorescence of the MIA probe also increased as well and resulted in declined net intensity. The result suggested that 100 μM the optimum dye concentration for the detection. The stability of the dyes against salt and photo irradiation has been assessed and shown in Fig. S3 (stability against photo irradiation) and Fig. S4 (stability against salt, NaCl). The three cyanines are generally photo-stable under the excitation of 488 nm. However, the fluorescence signals of the dye-labeled proteins are salt concentration dependent. The higher the salt concentration of NaCl added, the lower the fluorescence intensity. The presence of salt would govern the dye-protein interaction and the solubility of the cyanine dye in the buffer solution. The effect of the magnetic nanoparticles on the fluorescence of the protein-dye complexes has been investigated as shown Fig S5. The magnetic nanoparticles did not influence on the resultant fluorescence signal on the dye labeled proteins.

Standard curve

To demonstrate the sensitivity of the developed assay, a calibration plot of the average net intensity as a function of the concentration of the target antigen was constructed under the optimal conditions mentioned above. Briefly, target antigen of concentration ranged from 0 to 20 pM, was incubated with 10 mg/mL Ab1-MNPs and 100 pM Ab2, at 37 °C. The resultant MIAs were then labeled with 100 μM **SLAce** (PSA), **SPAce** (AFP), and **VLAce** (CEA). By measuring the fluorescence intensity of 50 individual MIAs as a function of target antigen concentration, the calibration curves (Fig. 3A-C) were achieved with a good linear correlation coefficient with R^2 = 0.996, R^2 = 0.991 and R^2 = 0.996 for **SLAce** labelled PSA composites, **SPAce** labelled AFP composites and **VLAce** labelled CEA composites, respectively. A limit of detection (LOD) for PSA 200 fM (6.5 pg/mL) (LOD = blank + 3 × standard error of mean of blank) and a limit of quantification of 2 pM (0.66 ng/mL) (LOQ = blank + 10 × standard error of mean of blank) were resulted. Moreover, the LOD for AFP and CEA was determined to be 300 fM and 600 fM respectively. With reference to the typically recognized serum cut-off value of PSA, AFP and CEA set at 4 ng/mL,[23, 24] 6 ng/mL (87 pM)[25] and 2.5 ng/mL (13.8 pM)[26] respectively, this detection assay is able to quantify the trace amount of cancer associated antigens in serum samples for clinical application. To further enhance the fluorescence signal given by the cyanine fluorophore, 10 % of glycerol was added to the MIAs. As studies showed that an increase in solvent viscosity will hinder the rotation of the molecular rotor and hence restrict the quenching pathway of the cyanine fluorophore leading to the fluorescence enhancement.[27] To demonstrate this phenomenon two calibration curves for the detection of PSA: with and without glycerol were constructed. As shown in Fig. 3D, the addition of the glycerol has almost doubled the fluorescence signal generated from the **SLAce** conjugated MIA. Although the addition of glycerol has also enhanced the background fluorescence signal (probe-only) and hence unable to significantly improve the detection limit, the presence of the glycerol can further enhance the sensitivity of the overall detection assay (the slope in Fig. 3D), suggesting that the addition of glycerol can facilitate the detection when a less sensitive detector, such as a conventional spectrofluorimeter, is used. To demonstrate the capability of point-of-care detection with conventional fluorimeter, a calibration curve of fluorescence intensity measured at 654 nm (emission wavelength of **SLAce** upon binding to protein) as a function of the PSA concentration has been constructed under the optimal conditions with 10% glycerol. As seen in Fig. S6, the assay has achieved a linear range from 0-200 pM of PSA with good linear correlation coefficient with R^2 = 0.962 and a LOD of 93 pM, which is below the serum cut-off value of PSA. It confirmed the feasibility of the assay for point-of-care detection with a conventional fluorimeter. The assay for the detection of protein biomarkers with TIRFM imaging system can provide a sensitive quantification with trace amount of sample, while the detection with commercial fluorimeter can facilitate a rapid and simple screening for protein biomarkers.

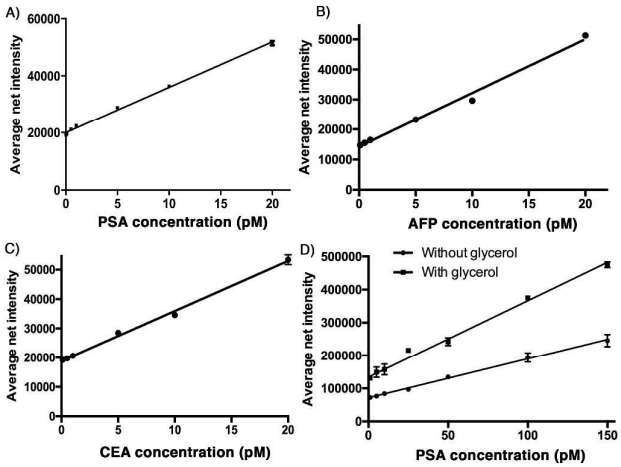

Fig. 3 Calibration plot for the quantification of PSA, A) different concentration of PSA were incubated with the probe and the labeling antibody, error bar, standard error of mean, n = 3. B) In the presence of 10% glycerol (top) and in the absence of 10% glycerol (bottom), error bar, standard error of mean, n = 3. (Average net intensity = (1×1 sq pixel of 50 individual MIAs) – (1×1 sq pixel of 50 individual background area on the image)/50)

Selectivity of the assay

Specificity of the detection probe plays an important role in the accuracy and the sensitivity of the detection assay. To demonstrate the selectivity of the developed assay, four different human antigens and protein samples (AFP, CEA, PSA and IgG) of a final concentration 10 pM were added and incubated with 10 mg/mL Ab1 conjugated nanoparticles and 100 pM Ab2 in the optimal conditions and labeled with 100 µM **SLAce**. IgG is the major component and the most abundant antibody isotype in human serum.[28, 29] The fluorescent images of MIAs were captured under the TIRFM imaging system. As illustrated in Fig. 4, the false hit rate in samples containing AFP, CEA and IgG was only 2.4 %, 6.3 % and 4.7 %, respectively (signal from sample – blank)/ (signal from PSA – blank) × 100 %). It indicated that the Ab1 conjugated nanoparticles and the Ab2 have a high binding affinity towards the target and capable of selectively discriminating target antigen from the others.

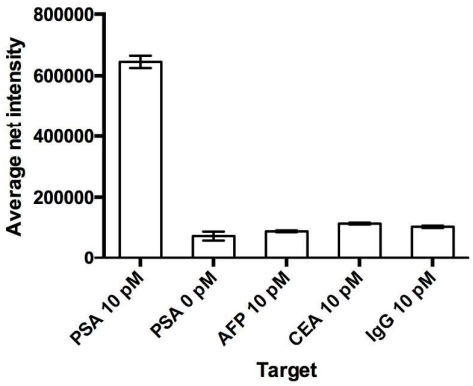

Fig. 4 Study of the selectivity of the assay. The probe is capable of differentiating the target from other proteins. Error bar, standard error of mean, n = 3. (Average net intensity = (1×1 sq pixel of 50 individual MIAs) – (1×1 sq pixel of 50 individual background area on the image)/50)

Detection of PSA in serum sample

To demonstrate the capability of quantifying the trace amount of antigen in serum sample, the developed system was applied to detect of PSA level in the crude serum sample of a healthy young male donor. An external calibration curve (Fig. 3A) was constructed for the determination of the serum PSA concentration. As illustrated in Fig. 5, the concentration of PSA in serum sample was found to be 14 pM. The result agreed very well with that obtained by the commercial available ELISA kit, which yielded 12.9 pM and far below the serum cut-off point of prostate cancer (122 pM). The developed assay thus provides a novel option for early cancer diagnosis.

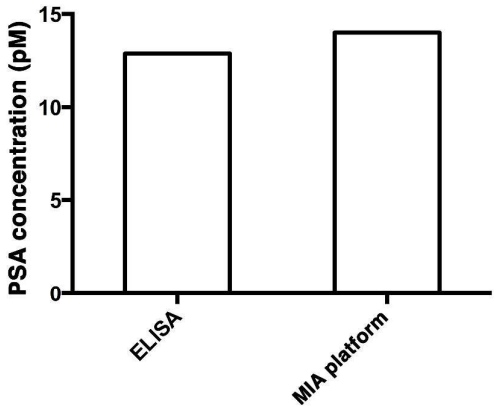

Fig. 5 Quantification of PSA in the crude serum sample by commercially available PSA ELISA kit (left) and MIA assay (right).

Simultaneous detection of cancer specific antigens in serum sample

To study the multiplexity of the detection assay, 10 pM of the target antigens, AFP, CEA, and PSA, were incubated with the corresponding Ab1-MNP probe and Ab2 in solution. Then the MIAs were further labeled with the tailor-made cyanine fluorophores, **SPAce**, **VLAce**, and **SLAce**, respectively. The solution mixture of the MIAs was then injected into the flow cell. The first-order fluorescent images were visualized under the TIRFM-EMCCD imaging system coupled with a transmission grating. As shown in Fig. 6, the **SPAce**-labeled AFP MIAs, **VLAce**-labeled CEA MIAs, and **SLAce**-labeled PSA MIAs exhibited emission peaks at 570 nm 650 nm, and 750 nm, respectively. The emission peaks matched with the emission bands of the corresponding cyanine fluorophores upon binding to PSA MIAs as shown in Fig. S7. From resolved spectra obtained from the first order images, the individual MIA was recognized and differentiated from one and other. The quantification of each of the target antigens was also achieved

by simply measuring the fluorescence signal of the corresponding MIAs.

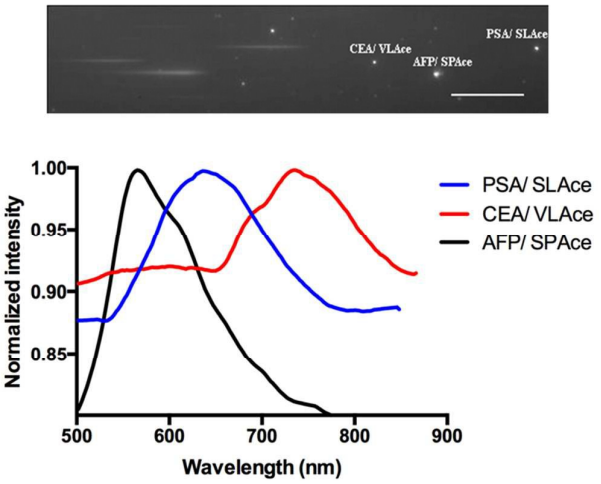

Fig. 6 Multiplex detection of the cancer associated antigens: zero and first order image of the immune-assemblies labeled with **SPAce**, **SLAce** and **VLAce**, respectively (top) and the corresponding emission spectra of magnetic immune-assemblies (bottom).

The assay was further applied to quantify the three cancer biomarkers in serum sample simultaneously. The MIAs capturing AFP, PSA and CEA were labeled with **SPAce**, **SLAce**, and **VLAce**, respectively. The concentration of the captured antigen from the sample was determined by measuring the peak intensity of the resolved spectra from first-order image of the nanocomposites. A standard curve was constructed as a reference (Fig. S8). As shown in Fig. 7, the expression profile of the AFP, PSA, and CEA in the crude serum was readily found to be of concentration 5.2 ± 0.014, 11 ± 0.023 and 0.27 ± 0.005 pM respectively. As the concentration of AFP and CEA detected is below the serum cut-off values, 6 ng/mL (87 pM)[25] and 2.5 ng/mL (13.8 pM)[26] and PSA concentration agreed with ELISA's and all the results are below the cut-off point of the corresponding cancer,[30-33] the system was demonstrated to be capable of simultaneous detection of three disease related antigens in 6 µL crude serum sample. We anticipated that any other protein biomarkers could be determined in the same manner for a more intensive expression profile and accurate disease diagnostics and prognostics.

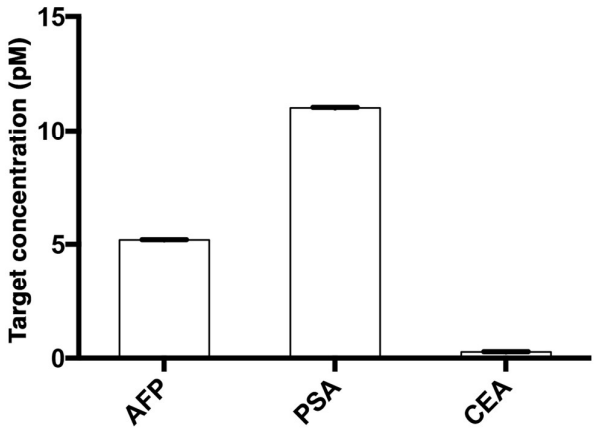

Fig. 7 Multiplex quantification of the cancer-associated antigens, AFP, PSA, CEA labeled with SPAce, SLAce and VLAce respectively.

Conclusions

In summary, a simple, direct, sensitive and specific assay for multiplex detection of disease-associated antigens using an antibody bio-conjugated magnetic probe and tailor-made turn-on fluorophores with TIRFM imaging system has been developed. The newly developed system is capable of selectively differentiating the target antigen from other proteins in the matrix and can achieve a remarkable LOD down to the femto-molar regime. This assay was further applied to quantify the amount of target cancer antigens in serum sample without sample enrichment and the results obtained agreed well with those of ELISA. The developed assay is of high potential to serve as an analytical tool for early disease diagnosis, progression monitoring and staging. Furthermore, this approach is universal and the as-developed assay can be readily modified and elaborated further, such as replacing the antibodies by other disease-associated antibodies, nucleic acid probes, or aptamers for a broad range of other biomedical research and disease diagnostics.

Acknowledgements

This work was financially supported by University Grants Council of Hong Kong Special Administrative Region, China (GRF/HKBU201612), Institute of Molecular Functional Materials which was supported by a grant from the University Grants Committee, Areas of Excellence Scheme (AoE/P-03/08) and the Young Scientists Fund from the National Science Foundation of China (21205006).

Notes and references

1. N. Kosaka, H. Iguchi and T. Ochiya, *Cancer Science*, 2010, **101**, 2087-2092.
2. R. R. S. Packard and P. Libby, *Clinical Chemistry*, 2008, **54**, 24-38.

3. L. M. Shaw, H. Vanderstichele, M. Knapik-Czajka, C. M. Clark, P. S. Aisen, R. C. Petersen, K. Blennow, H. Soares, A. Simon, P. Lewczuk, R. Dean, E. Siemers, W. Potter, V. M. Y. Lee, J. Q. Trojanowski and I. Alzheimer's Dis Neuroimaging, *Annals of Neurology*, 2009, **65**, 403-413.
4. C. A. K. Borrebaeck and C. Wingren, *Journal of Proteomics*, 2009, **72**, 928-935.
5. R. Chen, S. Pan, T. A. Brentnall and R. Aebersold, *Molecular & Cellular Proteomics*, 2005, **4**, 523-533.
6. E. Schiffer, H. Mischak and J. Novak, *Proteomics*, 2006, **6**, 5615-5627.
7. N. Spielmann and D. T. Wong, *Oral Diseases*, 2011, **17**, 345-354.
8. D. L. Adams, S. S. Martin, R. K. Alpaugh, M. Charpentier, S. Tsai, R. C. Bergan, I. M. Ogden, W. Catalona, S. Chumsri, C.-M. Tang and M. Cristofanilli, *Proceedings of the National Academy of Sciences of the United States of America*, 2014, **111**, 3514-3519.
9. S. S. Agasti, M. Liong, V. M. Peterson, H. Lee and R. Weissleder, *Journal of the American Chemical Society*, 2012, **134**, 18499-18502.
10. S. G. Baker, *Journal of the National Cancer Institute*, 2009, **101**, 1116-1119.
11. S. G. Baker, B. S. Kramer, M. McIntosh, B. H. Patterson, Y. Shyr and S. Skates, *Clinical Trials*, 2006, **3**, 43-56.
12. S. Bi, H. Zhou and S. Zhang, *Biosensors & Bioelectronics*, 2009, **24**, 2961-2966.
13. H. Wang, J. Wang, D. Choi, Z. Tang, H. Wu and Y. Lin, *Biosensors & Bioelectronics*, 2009, **24**, 2377-2383.
14. X. J. Feng, P. L. Wu, F. Bolze, H. W. C. Leung, K. F. Li, N. K. Mak, D. W. J. Kwong, J.-F. Nicoud, K. W. Cheah and M. S. Wong, *Organic Letters*, 2010, **12**, 2194-2197.
15. W. Yang, Y. Wong, O. T. W. Ng, L.-P. Bai, D. W. J. Kwong, Y. Ke, Z.-H. Jiang, H.-W. Li, K. K. L. Yung and M. S. Wong, *Angewandte Chemie-International Edition*, 2012, **51**, 1804-1810.
16. S.-H. Huang and R.-S. Juang, *Journal of Nanoparticle Research*, 2011, **13**, 4411-4430.
17. M. Namdeo, S. Saxena, R. Tankhiwale, M. Bajpai, Y. M. Mohan and S. K. Bajpai, *Journal of Nanoscience and Nanotechnology*, 2008, **8**, 3247-3271.
18. S. Prijic and G. Sersa, *Radiology and Oncology*, 2011, **45**, 1-16.
19. R. Bei and G. J. Mizejewski, *Current Molecular Medicine*, 2011, **11**, 564-581.
20. E. N. Debruyne and J. R. Delanghe, *Clinica Chimica Acta*, 2008, **395**, 19-26.
21. R. C. Bast, P. Ravdin, D. F. Hayes, S. Bates, H. Fritsche, J. M. Jessup, N. Kemeny, G. Y. Locker, R. G. Mennel, M. R. Somerfield and M. Amer Soc Clinical Oncology Tumor, *Journal of Clinical Oncology*, 2001, **19**, 1865-1878.
22. E. D. Crawford, C. L. Bennett, G. L. Andriole, M. B. Garnick and D. P. Petrylak, *Bju International*, 2013, **112**, 548-560.
23. A. Haese, A. de la Taille, H. van Poppel, M. Marberger, A. Stenzl, P. F. A. Mulders, H. Huland, C.-C. Abbou, M. Remzi, M. Tinzl, S. Feyerabend, A. B. Stillebroer, M. P. M. Q. van Gils and J. A. Schalken, *European Urology*, 2008, **54**, 1081-1088.
24. U. H. Stenman, M. Hakama, P. Knekt, A. Aromaa, L. Teppo and J. Leinonen, *Lancet*, 1994, **344**, 1594-1598.
25. G. L. H. Wong, H. L. Y. Chan, Y.-K. Tse, H.-Y. Chan, C.-H. Tse, A. O. S. Lo and V. W. S. Wong, *Hepatology*, 2014, **59**, 986-995.
26. M. J. Duffy, *Clin. Chem.*, 2001, **47**, 624-630.
27. F. Liu, T. Wu, M.-M. Hu, X.-J. Peng and J.-L. Fan, *Chemical Journal of Chinese Universities-Chinese*, 2012, **33**, 2239-2243.
28. R. Lemieux and R. Bazin, *Current Pharmaceutical Design*, 2006, **12**, 173-179.
29. R. Nezlin, *Immunology Letters*, 2009, **122**, 141-144.
30. J. Y. Choi, S. W. Jung, H. Y. Kim, M. Kim, Y. Kim, D. G. Kim and E. J. Oh, *World Journal of Gastroenterology*, 2013, **19**, 339-346.
31. H. Toyoda, T. Kumada, T. Tada, Y. Kaneoka, A. Maeda, F. Kanke and S. Satomura, *Cancer Science*, 2011, **102**, 1025-1031.
32. H. Korner, K. Soreide, P. J. Stokkeland and J. A. Soreide, *Annals of Surgical Oncology*, 2007, **14**, 417-423.
33. A. Nicolini, G. Tartarelli, A. Carpi, M. R. Metelli, P. Ferrari, L. Anselmi, M. Conte, P. Berti and P. Miccoli, *Bmc Cancer*, 2006, **6**.